Optimization of 3D-printed microstructures for investigating the properties of the mucus biobarrier

Bunea, Ada-Ioana; Jakobsen, Mogens Havsteen; Engay, Einstom; Bañas, Andrew Rafael; Glückstad, Jesper

Published in:
Micro and Nano Engineering

Link to article, DOI:
10.1016/j.mne.2018.12.004

Publication date:
2019

Document Version
Publisher's PDF, also known as Version of record

Micro and Nano Engineering 2 (2019) 41–47

Contents lists available at ScienceDirect

Micro and Nano Engineering

journal homepage: www.elsevier.com/locate/tsf

Optimization of 3D-printed microstructures for investigating the properties of the mucus biobarrier

Ada-Ioana Bunea [a,*], Mogens Havsteen Jakobsen [b], Einstom Engay [a], Andrew R. Bañas [a], Jesper Glückstad [a]

[a] Department of Photonics Engineering, DTU Fotonik, Lyngby DK-2800, Denmark
[b] Department of Micro- and Nanotechnology, DTU Nanotech, Lyngby DK-2800, Denmark

ARTICLE INFO

Article history:
Received 18 October 2018
Received in revised form 30 November 2018
Accepted 17 December 2018
Available online xxxx

Keywords:
Optical catapulting
Two-photon polymerization
Surface modification
Generalized Phase Contrast
Light Robotics
Mucus biobarrier

ABSTRACT

In order to overcome the mucus biobarrier for drug delivery purposes, a better understanding of the interactions between mucus and the drug carrier is needed. We propose optical catapulting of 3D-printed microstructures with tailored shape and surface chemistry as a means to study the interaction filtering properties of a model mucus biobarrier in dynamic conditions. Using two-photon polymerization, we fabricate microstructures with a resolution of approximately 200 nm. We introduce amino functional groups on the surface of the IP-L 780-derived polymer in a single step process via UV-assisted functionalization with an anthraquinone amine photolinker. Our optical catapulting system relies on Generalized Phase Contrast for beam shaping and it allows us to manipulate microstructures over a distance of 250 μm, similar to the mucus layer thickness in the upper part of the lower human intestine. This work is part of an ongoing endeavor to establish Light Robotics as a valuable toolbox for biomedical research.

1. Introduction

Oral administration of a large number of biopharmaceuticals has proven challenging due to severe limitations in their bioavailability caused by degradation in the gastrointestinal (GI) tract, poor permeation through the intestinal barrier and systemic distribution [1]. In particular, peptides, proteins and a number of vaccines suffer from low oral bioavailability [1–4]. However, oral administration is a convenient, pain-free route for the patient and reduces the need for specialized personnel. Therefore, understanding and overcoming the challenges posed by oral administration of selected biopharmaceuticals has been in focus in recent years.

For successful drug delivery upon oral administration, the active molecule needs to survive the acidic environment of the stomach and to penetrate the intestinal biobarrier consisting in the GI tract mucus [1,5] and the intestinal epithelium, a monolayer of epithelial cells connected by tight junctions [6]. The internal surfaces of the GI tract are covered by a dynamic semipermeable mucus layer composed mainly of mucins secreted by goblet cells present in the intestinal epithelium [7–10]. Mucus functions both as a lubricant and as a barrier in the GI tract, facilitating the passage of food during digestion and preventing toxins and pathogens from reaching the epithelial surfaces. The mucus pore mesh enables size filtering, while the chemical properties of the mucus facilitate interaction filtering, meaning that only small particles with certain surface chemistry can penetrate the mucus biobarrier.

Mucus typically consists of 2–5% (*w*/*v*) mucins and small amounts of other proteins, lipids and electrolytes [9,11]. The thickness and composition of the GI mucus layer varies considerably between individuals and along the GI tract, with average values in the small intestine ranging from 125 to 480 μm [11]. Drug delivery of nanoparticles through mucus requires tailoring the surface chemistry of the particles towards either mucoadhesion or mucopenetration [5,12]. Thus, understanding the interaction between the particles and the mucus biobarrier represents an important step for designing drug delivery systems capable of penetrating the mucus layer and reaching the intestinal epithelium. As a means to study this interaction in a dynamic system, we propose optical catapulting of microstructures with tailored shapes and surface chemistry. Due to the micrometer-size of our structures, they are not suitable for investigating the size filtering properties of the mucus mesh. However, our microstructures should allow us to gain information on the interaction filtering properties of mucus, based on e.g. hydrogen bonding, hydrophobic and ionic interactions [13]. This can be achieved through chemical immobilization of various molecules on the surface of the microstructures. Furthermore, the influence of the particle shape in the interaction with mucus models will be investigated.

Two-photon polymerization (2PP) is the highest resolution available 3D-printing method [14,15], allowing direct laser writing of structures with a resolution of ~200 nm, which can be further improved by post-processing [16] or by additional control over the polymerization process

* Corresponding author.
E-mail address: adabu@fotonik.dtu.dk (A.-I. Bunea).

https://doi.org/10.1016/j.mne.2018.12.004

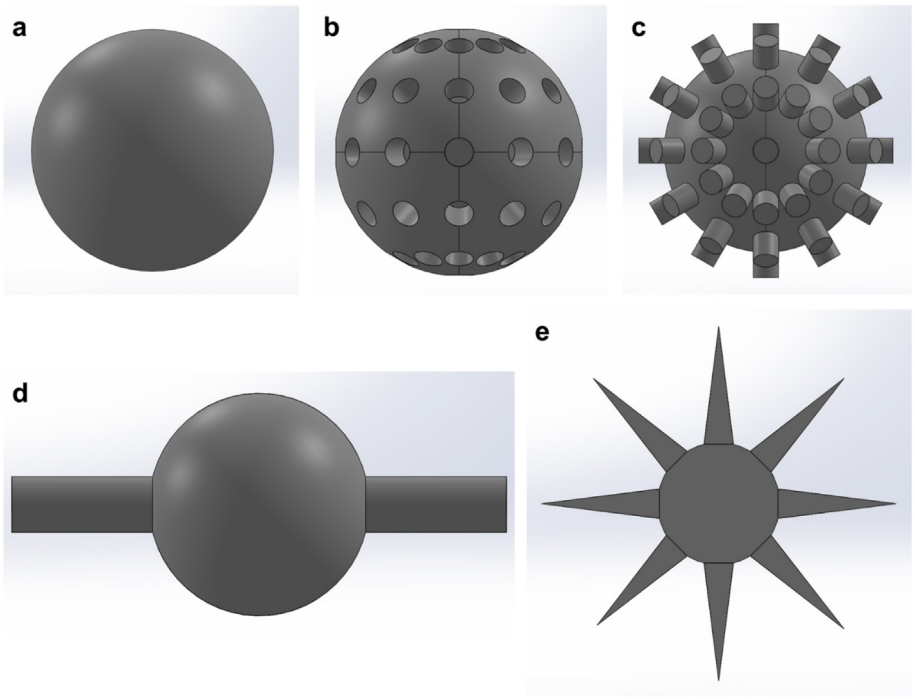

Fig. 1. Investigated designs. The radius of the sphere is (a) 8.3 μm; (b) 8.6 μm; (c-e) 8 μm.

[17]. The advantages of 2PP have made it an important tool for fabricating microstructures with defined shapes tailored to specific applications. This includes microtools amenable to optical manipulation that fall under the umbrella of Light Robotics [18–21], an emerging field in which our group is one of the pioneers. In addition to shape optimization, control over the surface chemistry properties of the microtools is important, especially for biosensing or biomedical research applications. Surface modification by selective metal coating is relatively well established [22–24]. Other functionalization approaches reported in literature for polymers processed using 2PP include acid catalysis followed by aminosilane incubation of SU-8 microstructures [25,26] or ethylene diamine Michael addition to acrylate groups present on Sartomer-derived polymers [27]. Although reasonably effective, these approaches for surface functionalization with amine groups require multiple steps and involve toxic chemicals. Functionalization via thiol-Michael addition reactions was also recently reported, but it required the in-house development of resins for 2PP [28,29].

The microstructures presented herein combine shape and surface optimization [30] with actuation via intelligently-sculpted light beams and are meant to further the Light Robotics toolbox by enabling insight into the mucus biobarrier for drug delivery studies. To the best of our knowledge, this represents the first report of surface modification of the polymer derived from the commercial Nanoscribe proprietary photoresist, IP-L 780. This was achieved by single-step UV-assisted photolinking of an antraquinone amine directly on the surface of the crosslinked resin.

2. Materials and methods

2.1. Fabrication

The microstructures were fabricated by direct laser writing (DLW) using two-photon polymerization (2PP). We used the negative-tone acrylic photoresist Nanoscribe IP-L 780 and a Nanoscribe Photonic Professional GT system (Nanoscribe GmbH, Germany) for printing on 170 μm thick glass substrates. The Nanoscribe system uses 150 fs pulses emitted at 100 MHz by a 780 nm Ti-Sapphire laser.

The 3D design was done in SolidWorks and the associated STL file was imported into Nanoscribe's DeScribe software, where the code required for 3D-printing was generated. The slicing and hatching distances were set to 200 nm and the power scaling was fixed to correspond to 16 mW average power at the aperture objective. The stage velocity was set to 200 $\mu m \cdot s^{-1}$. After 3D-printing, the structures were developed by 20 min incubation in isopropanol, rinsed with Millipore water (18.2 MΩ·cm at 25 °C) and blow-dried with air.

For testing and characterizing surface modification, large flat structures were prepared by dropcasting the IP-L 780 photoresist on 170 μm thick glass substrates, followed by overnight soft bake at room temperature. Crosslinking was achieved by 15 min exposure to ultraviolet (UV) light in a homemade UV-box containing HPA lamps with emission in the range of 330 to 380 nm, peaking at 365 nm, 18 $mW \cdot cm^{-2}$ (PHILIPS, Netherlands). The flat structures were developed by 20 min incubation in isopropanol, rinsed with Millipore water and blow-dried with air.

Table 1
Parameters of the tested designs. All microstructures have a volume of ~ $2.4 \cdot 10^{-9}$ cm^3 after printing.

Design	Feature	No. of features	Sphere radius (μm)	Feature size (μm)	Total surface area (cm^2)	Surface area increase[a] (%)
a	None	N/A	8.3	N/A	$8.7 \cdot 10^{-6}$	N/A
b	Cylinder	62	8.6	$r = 1$, h = 1	$13.2 \cdot 10^{-6}$	50
c	Cylinder	62	8	r = 1, h = 1	$11.9 \cdot 10^{-6}$	35
d	Cylinder	2	8	$r = 2$, h = 10	$10.5 \cdot 10^{-6}$	20
e	Cone	8	8	$r = 1.5$, h = 12	$12.2 \cdot 10^{-6}$	40

[a] The surface area increase is given in percentage form in relation to the surface area of the simple sphere design a.

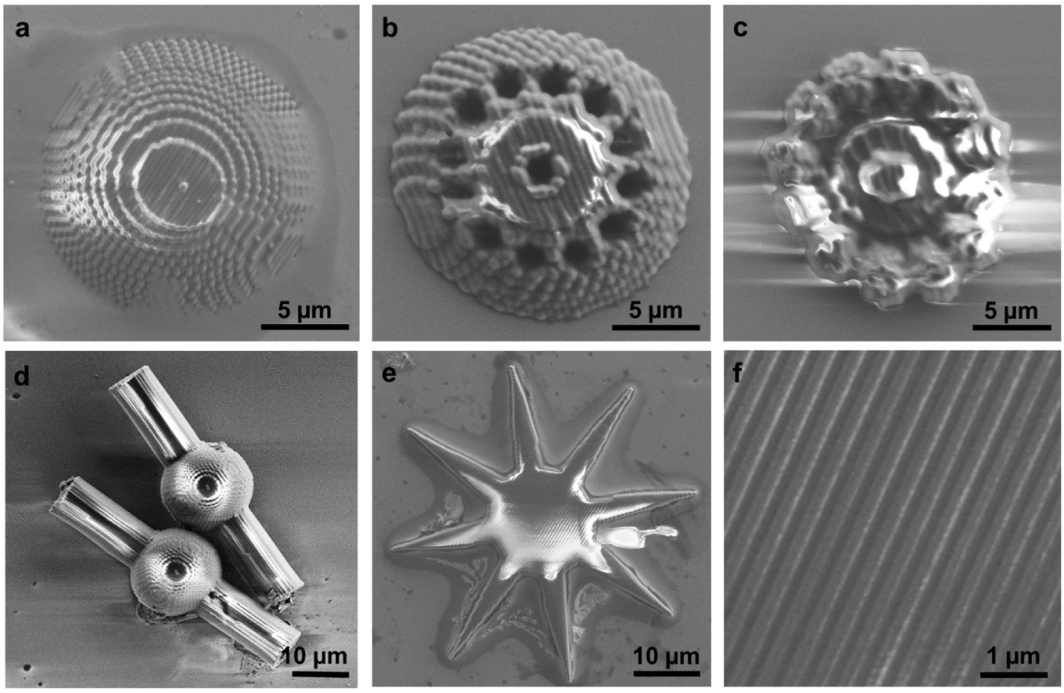

Fig. 2. (a-e) SEM images of the 3D-printed microstructures. (f) Enlarged area where the print lines are clearly visible. Images such as this were used to determine the printing resolution.

2.2. Surface modification

The anthraquinone amine hydrochloride (AQ-amine, (H-βAla-βAla-NH-$(CH_2)_3$-NHCO-AQ · HCl), molecular weight 486.96 $g \cdot mol^{-1}$) was synthesized as described in [31]. The AQ-amine was dissolved in water at a concentration of 0.5 mM. 300 μL of AQ-amine solution were dropcast on top of the flat surfaces and exposed to UV light for 5, 10 or 15 min. The exposure time needs to be adjusted for to achieve optimal surface modification. After UV exposure, the samples were rinsed with Millipore water, blow-dried with air and stored in a closed Petri dish, protected from light, until characterization.

2.3. Scanning electron microscopy

Scanning Electron Microscopy (SEM) was performed using a Zeiss Supra 40 VP SEM (ZEISS, Germany). SEM images were acquired from a secondary electron detector using an accelerating voltage (EHT) of 1.5 kV in high vacuum mode. High magnification SEM images where the print lines were clearly visible were used for determining the print resolution. The appropriate pixel size was defined in the ImageJ software [32] for each SEM image used for this purpose. The "Measure" tool in the ImageJ software was then used to determine the distance between two adjacent print lines and therefore the resolution. 30 total measurements were performed on 6 different samples, giving an average distance of 194 ± 23 μm between adjacent print lines.

2.4. X-ray photoelectron spectroscopy

X-ray photoelectron spectroscopy (XPS) was performed using a ThermoScientific K-alpha XPS (Thermo Fisher Scientific, MA, USA). Three distinct areas of three different samples were analyzed for the data presented herein.

2.5. Fourier-transform infrared spectroscopy

Fourier-transform infrared spectroscopy (FT-IR) was performed using a Spectrum 100 FT-IR Spectrometer (Perkin Elmer, MA, USA). Air was used as baseline. Each spectrum was acquired as an accumulation of three scans between 4000 and 650 cm^{-1} using the Attenuated Total Reflection (ATR) Element.

2.6. Mucus model

Type II porcine gastric mucin (cat. no. M2378) and 1 M HEPES (cat. no. H0887, pH 7.0–7.6) were purchased from Sigma-Aldrich Denmark A/S. Tween 80 (cat. no. 02103170) was purchased from MP Biomedicals (CA, USA). The 1 M HEPES buffer was diluted to 10 mM using Millipore water.

Our simple mucus model consisted in 5% type II porcine gastric mucin (PGM) reconstituted in 10 mM HEPES buffer containing 0.1% Tween 80. The mucus model was prepared by adding dry PGM to a 10 mM HEPES buffer containing 0.1% Tween 80 and allowing it to rehydrate for 20 min at room temperature under gentle stirring (300 rpm).

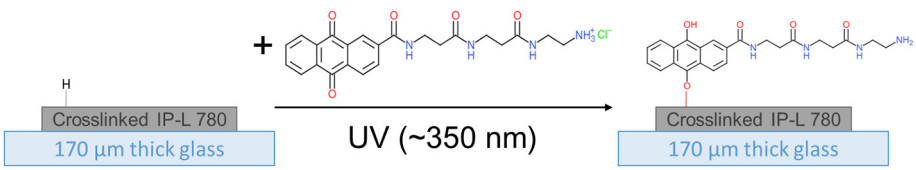

Fig. 3. Schematic of UV-assisted surface modification of IP-L 780-derived polymer with anthraquinone amine.

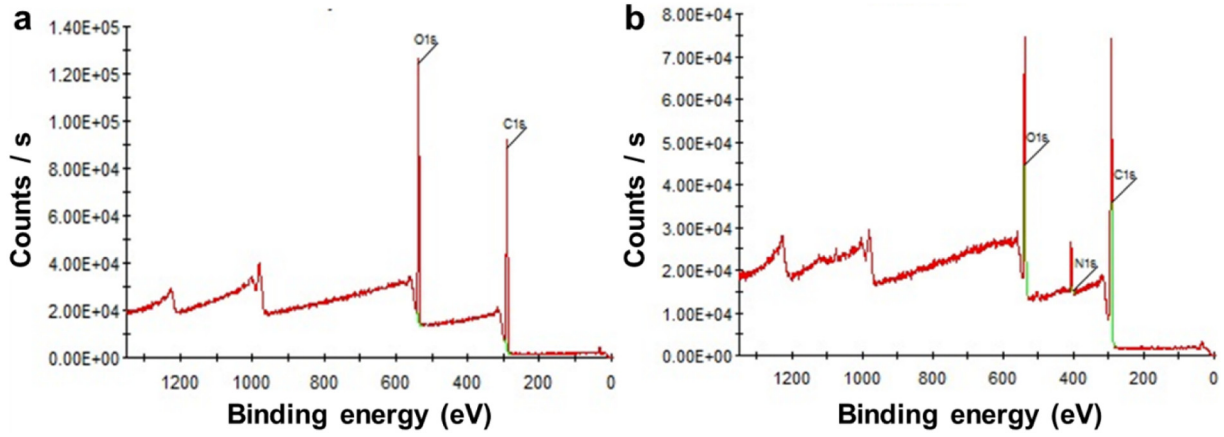

Fig. 4. (a, b) Typical XPS survey spectra of IP-L 780 photoresist after (a) crosslinking and (b) surface modification with anthraquinone amine. The presence of nitrogen after surface modification indicates that the surface has been functionalized.

2.7. Optical catapulting

The optical catapulting setup is described in detail elsewhere (under review). A 1070 nm laser (IPG Photonics, MA, USA) shaped by a Generalized Phase Contrast (GPC) system was used for catapulting. A LCoS type spatial light modulator (SLM) (Hamamatsu Photonics, Japan) with 800 × 600 pixels with a pixel pitch of 20 μm was used to actuate the shaped GPC output via a "Holo-GPC" configuration [33]. The laser was demagnified to have a 1 mm diameter in order to match a premade GPC light shaper [34]. The Fourier transform of the illuminated phase mask was expanded onto the SLM by 5× by placing a lens (f = 250 mm) after the GPC light shaper. The distribution at the SLM was subsequently demagnified onto the back aperture of the objective lens by 1/3× using a pair of lenses ($f_1 = 300$ mm and $f_2 = 100$ mm). Two objective lenses (f = 3.6 mm, NA = 0.55) were used to image the GPC disks onto the sample and for top view imaging, while a third objective lens (f = 45 mm, NA = 0.1) was employed for the side view imaging. The resulting disk after the f = 3.6 mm objective lens had a calculated diameter of ~17 μm. The top view was necessary for aligning the system and ensuring that the beam was directed at the microstructures to be catapulted. Data for particle tracking was acquired through side view imaging.

For the preliminary optical catapulting results mentioned herein, Polybead polystyrene microspheres (Polysciences Inc., PA, USA) with a radius of 7.5 μm were employed. The microspheres (1.5%) were added to the mucus model immediately after preparation and transferred to a quartz cuvette with a 250 × 250 μm^2 channel (Hellma GmbH, Germany). Reference experiments were performed using Millipore water instead of the mucus model.

2.8. Particle tracking

The motion of the microspheres in the measurement chamber was recorded with a Point Grey camera (Basler, AG, Germany) at 10 fps. Particle tracking was performed using the Manual Tracking plugin for the ImageJ software [32]. The accuracy of the tracking is limited by the pixel size to approximately 0.1 μm. Trajectories were computed by tracking catapulted microspheres from the first frame in which they rise above the lower cuvette wall until the last frame just before reaching the upper cuvette wall. The visual representation of the trajectories is given by the Dots and lines option in the Manual Tracking plugin. The trajectories are approximately 250 μm long, as defined by the measurement chamber height.

3. Results and discussion

3.1. Shape optimization

Five different designs were made, starting from a simple sphere, which facilitates optical catapulting (Fig. 1). All the microtools were designed to have the same volume, and therefore also the same weight, after printing. It is important to maintain the same weight for all the

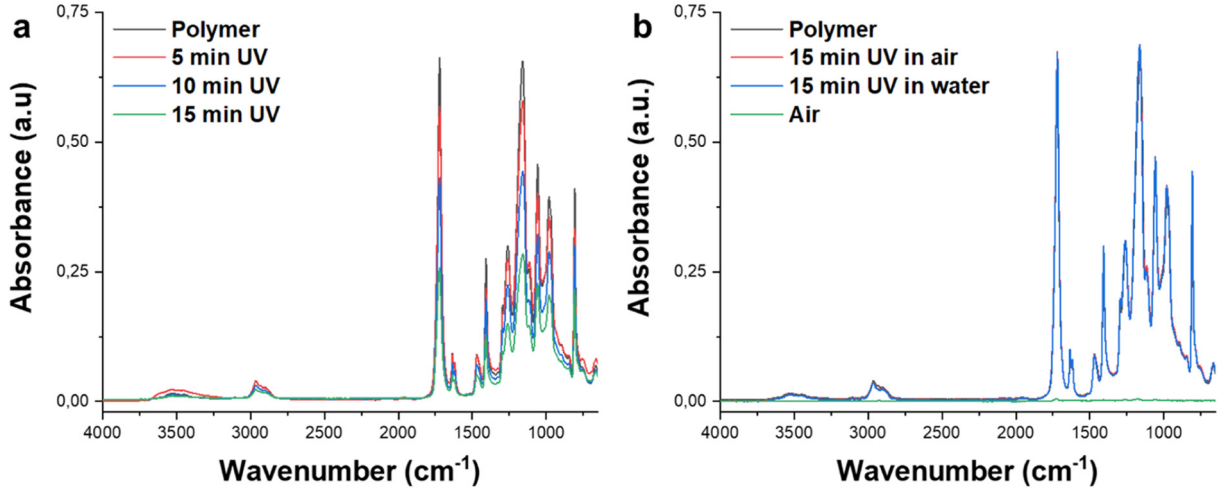

Fig. 5. FT-IR absorbance spectra in Attenuated Total Reflection mode of (a) IP-L 780-derived polymer and polymer modified with anthraquinone amine using different UV exposure times; (b) reference samples: air, crosslinked polymer, polymer exposed to 15 min UV in air, and polymer exposed to 15 min UV in water.

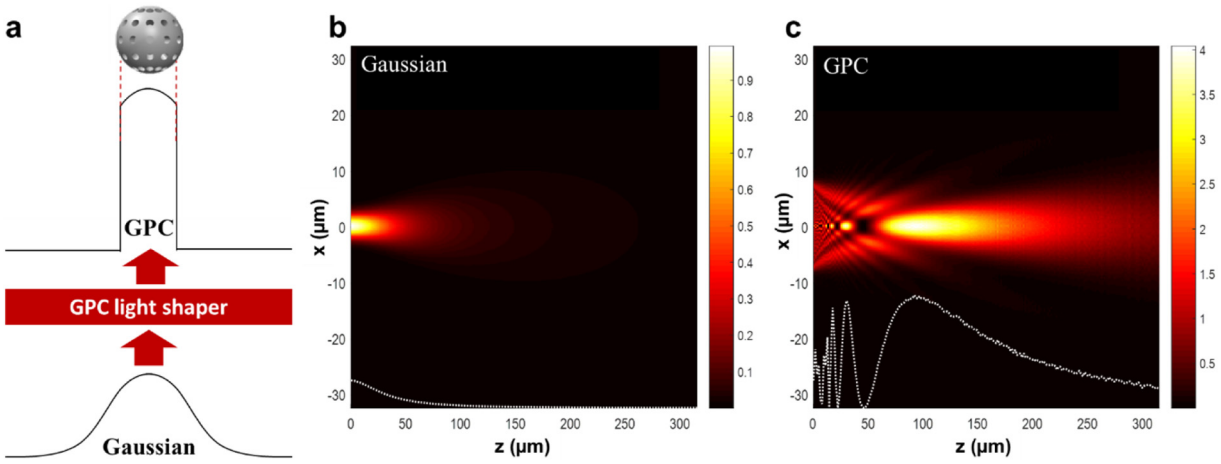

Fig. 6. Generalized Phase Contrast (GPC) light-shaping for optical catapulting. (a) Using GPC, a Gaussian beam from the infrared laser source is shaped to match the particle diameter in order to maximize efficiency and obtain a relatively uniform light distribution on the particle. (b, c) Pseudo-color plots of the xz plane intensity distribution for (b) Gaussian and (c) GPC-shaped beams directed towards the positive z-axis simulated with the constrain that their energy falls within the same region, corresponding to a particle to be catapulted [42].

microstructures in order to be able to compare the velocities of the particles during catapulting while neglecting the influence of gravitational forces. The volume after printing is of approximately $2.4 \cdot 10^{-9}$ cm^3 for all the tested designs. The parameters of the five designs are shown in Table 1.

The designed microstructures have surface areas increased by 20–50% compared to their spherical base due to the features included. This should facilitate an increase in the amount of chemical modifier that can be attached to the surface. Furthermore, the microstructures are expected to have different hydrodynamic behavior due to their different shapes.

SEM imaging of the polymeric microstructures is challenging, as the samples are non-conductive and tend to charge during imaging. However, it was possible to image the samples with sufficient resolution by using a relatively low accelerating voltage (1.5 kV) and the secondary electron detector. SEM images of the microstructures are shown in Fig. 2. The resolution of our printing method, as determined from SEM images, is approximately 200 nm, in good agreement with the producer specifications for the IP-L 780 photoresist.

3.2. Surface modification

The schematic mechanism of the covalent surface modification with the AQ-amine photolinker is shown in Fig. 3. Anthraquinones are easily excited with soft UV light. The excited anthraquinone species is highly reactive and reacts with almost any C—H containing polymer. In the first step, the excited anthraquinone extracts a hydrogen atom from the polymer surface. Subsequently, the formed hydroquinone combines with the polymer surface radical, resulting in a covalent ether bond [35,36].

The IP-L 780 photoresist is an acrylic resin. The polymer obtained after crosslinking contains carbon, oxygen and hydrogen. A typical XPS survey spectrum of IP-L 780 crosslinked by 15 min UV irradiation is shown in Fig. 4a. No nitrogen is present on the surface of the unmodified polymer. The AQ-amine employed was grafted directly on the polymer surface by UV irradiation. A typical XPS survey spectrum obtained after surface modification is shown in Fig. 4b. The presence of nitrogen on the surface after treatment with UV in the presence of AQ-amine solution confirms the successful attachment of the photolinker on the surface. The AQ-amine grafting is dose dependent, showing an increase in surface nitrogen from 0.3 ± 0.1% (after 5 min UV exposure) to 1.5 ± 0.6% (after 10 min exposure) and 3.1 ± 0.5% (after 15 min exposure), as calculated from the survey scans. Further increasing the exposure time might lead to improved grafting of the AQ-amine photolinker.

FT-IR spectra of the polymer were acquired for the different UV exposure doses tested (Fig. 5). Significant changes can be observed upon UV exposure in the presence of the photolinker (Fig. 5a), confirming

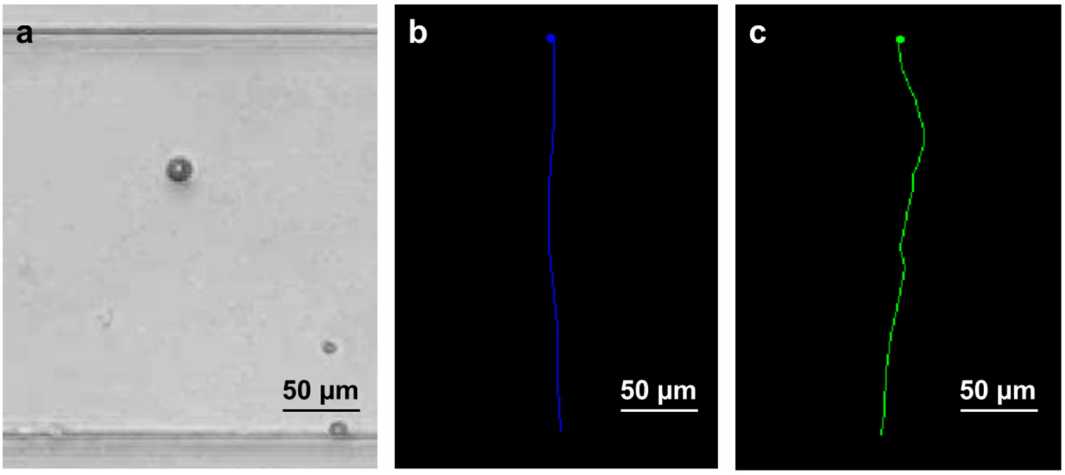

Fig. 7. (a) Still frame from a video recording of a polystyrene microsphere being catapulted in water. During each catapulting experiment, one microsphere is pushed using GPC-shaped light from the bottom to the top of the measurement cuvette, over a distance of 250 μm. The microsphere trajectory is then determined and analyzed. (b, c): Microsphere trajectories recorded using a laser input power of 1 W in (b) water and (c) 5% mucus model.

the observations from XPS. To ensure that the observed changes in the FT-IR spectra are caused by the photolinker and not by UV exposure, reference samples were prepared and exposed to UV as such or after adding Millipore water on the surface. As shown by the reference measurements, UV exposure does not cause changes in the FT-IR spectra in the absence of anthraquinone amine (Fig. 5b).

3.3. Mucus model

Mucus models are widely used in research due to the scarcity and low stability of native mucus GI samples. The simplest, widely-used, viable mucus models are rehydrated porcine gastric mucin (PGM) dispersions [37]. Rehydrated PGM mucus models poorly match the viscoelastic properties of native mucus due to glycoprotein chain scission during the dehydration step [38]. Thus, the simple mucus model employed in this study would not be suitable for studying the size filtering properties of human mucus. However, the physicochemical properties of PGM closely resemble those of human mucins [39,40], which makes the model adequate for investigating the interaction filtering properties, while minimizing steric hindrance.

3.4. Optical catapulting

To match the mucus thickness in the upper small intestine, a straight microfluidic chamber with a height of 250 μm was employed. Microspheres mixed in the PGM mucus model were deposited inside the chamber and employed in optical catapulting experiments.

Laser light from a 1070 nm infrared laser source was shaped using Generalized Phase Contrast (GPC). The GPC light shaper turns an input beam from the laser, which is characterized by a Gaussian intensity distribution, into an output beam with a characteristic top-hat profile (Fig. 6a). GPC was preferred as light shaping method for the optical catapulting setup, as it offers several advantages: i) efficient use of laser power [41–43], ii) relatively-uniform intensity distribution on the particle and iii) extended beam profile suitable for providing consistent force to the particle over extended distances [44–46](Fig. 6c).

Preliminary experiments using 15 μm polystyrene microspheres showed that the optical catapulting setup described is able to propel particles in a 5% PGM mucus model using input laser powers starting from 0.5 W (under review elsewhere). Velocities of up to 100 $\mu m \cdot s^{-1}$ were achieved by increasing the laser input power to 1.8 W. By adjusting the laser input power, the ability of the particles to penetrate the model biobarrier can be controlled.

Fig. 7 shows a frame from a video of a microsphere being catapulted in water and particle trajectories recorded in water and the mucus model. Microspheres catapulted in water tend to follow a linear path (Fig. 7b). The microspheres move significantly slower in the mucus model compared to water (under review elsewhere). Furthermore, in the mucus model, the microspheres follow paths that clearly deviate from linearity (Fig. 7c). This is most likely determined by the hydrophobic interactions between the microspheres and the mucins present in the model biobarrier. Based on these preliminary observations, it is to be expected that both the velocities and the particle trajectories will be influenced by the shape and surface chemistry of the microstructures This could be used to gain information about the particle – mucus model interactions.

4. Conclusions and perspectives

Microstructures for optical catapulting were designed and fabricated using two-photon polymerization. Primary amine functional groups were introduced on the surface of the IP-L 780 derived polymer using an anthraquinone amine photolinker in a single step process. The UV-assisted surface modification was characterized using XPS and FT-IR and was found to be dose dependent, with a 15 min UV exposure time giving better results than lower exposure times. Additional optimization of the surface modification process can be done in terms of exposure dose, AQ-amine concentration or solvent employed during functionalization. Optimizing all aforementioned parameters should lead to maximum surface coverage with the AQ-amine photolinker.

The presence of primary amine groups on the surface facilitates further surface modification with a wide range of molecules that can give e.g. mucoadhesive or mucopenetrant properties to the microstructures. To the best of our knowledge, this is the first time that surface functionalization of IP-L 780 derived polymer is reported.

The optical setup is able to propel microstructures through a simple mucus model with velocities of up to100 $\mu m \cdot s^{-1}$. The laser power can be adjusted to ensure that the particles can be translated vertically over 250 μm through the mucus model.

The influence of the particle shape and various surface modifiers on microparticle motion through the mucus model will be explored in further studies. Particle tracking will be employed to gain information about i) the velocity and ii) the path of microstructures travelling through the mucus model. A high velocity and/or a linear trajectory should mean that the microstructure is able to move easily through the mucus model. Optical catapulting could become a dynamic characterization method able to complement existing techniques used to study interactions, such as quartz crystal microbalance (QCM). This should allow valuable insight into the interaction filtering properties of mucus biobarriers.

Acknowledgements

Special thanks go to Manto Chouliara for her help with optical catapulting experiments, to Dr. Paul Mines for his help with FT-IR and to Prof. Hanne Mørck Nielsen for fruitful discussions. We acknowledge funding from the Novo Nordisk Foundation (Grand Challenge Program NNF16OC0021948) and VILLUM FONDEN (Research Grant 00022918).

We declare no conflicts of interest.

References

[1] B.F. Choonara, Y.E. Choonara, P. Kumar, D. Bijukumar, L.C. du Toit, V. Pillay, A review of advanced oral drug delivery technologies facilitating the protection and absorption of protein and peptide molecules, Biotechnol. Adv. 32 (2014) 1269–1282, https://doi.org/10.1016/J.BIOTECHADV.2014.07.006.

[2] S. Rosales-Mendoza, C. Angulo, B. Meza, Food-grade organisms as vaccine biofactories and oral delivery vehicles, Trends Biotechnol. 34 (2016) 124–136, https://doi.org/10.1016/J.TIBTECH.2015.11.007.

[3] A. Vos, C.M. Freuling, B. Hundt, C. Kaiser, S. Nemitz, A. Neubert, T. Nolden, J.P. Teifke, V. te Kamp, R. Ulrich, S. Finke, T. Müller, Oral vaccination of wildlife against rabies: differences among host species in vaccine uptake efficiency, Vaccine 35 (2017) 3938–3944, https://doi.org/10.1016/J.VACCINE.2017.06.022.

[4] V. Truong-Le, P.M. Lovalenti, A.M. Abdul-Fattah, Stabilization challenges and formulation strategies associated with oral biologic drug delivery systems, Adv. Drug Deliv. Rev. 93 (2015) 95–108, https://doi.org/10.1016/j.addr.2015.08.001.

[5] L.M. Ensign, R. Cone, J. Hanes, Oral drug delivery with polymeric nanoparticles: the gastrointestinal mucus barriers, Adv. Drug Deliv. Rev. 64 (2012) 557–570, https://doi.org/10.1016/J.ADDR.2011.12.009.

[6] L.W. Peterson, D. Artis, Intestinal epithelial cells: regulators of barrier function and immune homeostasis, Nat. Rev. Immunol. 14 (2014) 141–153, https://doi.org/10.1038/nri3608.

[7] R.A. Cone, Barrier properties of mucus, Adv. Drug Deliv. Rev. 61 (2009) 75–85, https://doi.org/10.1016/j.addr.2008.09.008.

[8] G.Y. Chen, T.S. Stappenbeck, Mucus, it is not just a static barrier, Sci. Signal. 7 (2014) pe11, https://doi.org/10.1126/scisignal.2005357.

[9] M. Boegh, H.M. Nielsen, Mucus as a barrier to drug delivery - Understanding and mimicking the barrier properties, Basic Clin. Pharmacol. Toxicol. 116 (2015) 179–186, https://doi.org/10.1111/bcpt.12342.

[10] M. García-Díaz, D. Birch, F. Wan, H.M. Nielsen, The role of mucus as an invisible cloak to transepithelial drug delivery by nanoparticles, Adv. Drug Deliv. Rev. 124 (2017) 107–124, https://doi.org/10.1016/j.addr.2017.11.002.

[11] R. Bansil, B.S. Turner, The biology of mucus: Composition, synthesis and organization, Adv. Drug Deliv. Rev. 124 (2017) 3–15, https://doi.org/10.1016/j.addr.2017.09.023.

[12] K. Maisel, L. Ensign, M. Reddy, R. Cone, J. Hanes, Effect of surface chemistry on nanoparticle interaction with gastrointestinal mucus and distribution in the gastrointestinal tract following oral and rectal administration in the mouse, J. Control. Release 197 (2015) 48–57, https://doi.org/10.1016/J.JCONREL.2014.10.026.

[13] S.P. Authimoolam, T.D. Dziubla, Biopolymeric mucin and synthetic polymer analogs: their structure, function and role in biomedical applications, Polymers (Basel). 8 (2016) 71, https://doi.org/10.3390/polym8030071.
[14] S. Kawata, H.-B. Sun, T. Tanaka, K. Takada, Finer features for functional microdevices, Nature 412 (2001) 697–698, https://doi.org/10.1038/35089130.
[15] J.-F. Xing, M.-L. Zheng, X.-M. Duan, Two-photon polymerization microfabrication of hydrogels: an advanced 3D printing technology for tissue engineering and drug delivery, Chem. Soc. Rev. 44 (2015) 5031–5039, https://doi.org/10.1039/C5CS00278H.
[16] G. Seniutinas, A. Weber, C. Padeste, I. Sakellari, M. Farsari, C. David, Beyond 100 nm resolution in 3D laser lithography — Post processing solutions, Microelectron. Eng. 191 (2018) 25–31, https://doi.org/10.1016/J.MEE.2018.01.018.
[17] S. Wang, Y. Yu, H. Liu, K.T.P. Lim, B.M. Srinivasan, Y.W. Zhang, J.K.W. Yang, Sub-10-nm suspended nano-web formation by direct laser writing, Nano Futur. 2 (2018) 025006, https://doi.org/10.1088/2399-1984/aabb94.
[18] J. Glückstad, D. Palima, Light Robotics : Structure-Mediated Nanobiophotonics, Elsevier, 2017.
[19] S. Nocentini, C. Parmeggiani, D. Martella, D.S. Wiersma, Optically driven soft micro robotics, Adv. Opt. Mater. 6 (2018) 1800207, https://doi.org/10.1002/adom.201800207.
[20] W. Lamperska, S. Drobczyński, M. Nawrot, P. Wasylczyk, J. Masajada, W. Lamperska, S. Drobczyński, M. Nawrot, P. Wasylczyk, J. Masajada, Micro-Dumbbells—a versatile tool for optical tweezers, Micromachines. 9 (2018) 277, https://doi.org/10.3390/mi9060277.
[21] H. Zeng, P. Wasylczyk, D.S. Wiersma, A. Priimagi, Light robots: bridging the gap between microrobotics and photomechanics in soft materials, Adv. Mater. 30 (2018) 1703554, https://doi.org/10.1002/adma.201703554.
[22] M.J. Villangca, D. Palima, A.R. Bañas, J. Glückstad, Light-driven micro-tool equipped with a syringe function, Light Sci. Appl. 5 (2016) e16148, https://doi.org/10.1038/lsa.2016.148.
[23] E. Engay, A.-I. Bunea, M. Chouliara, A. Bañas, J. Glückstad, Natural convection induced by an optically fabricated and actuated microtool with a thermoplasmonic disk, Opt. Lett. 43 (2018) 3870–3873, https://doi.org/10.1364/OL.43.003870.
[24] Y.-S. Chen, A. Tal, D.B. Torrance, S.M. Kuebler, Fabrication and characterization of three-dimensional silver-coated polymeric microstructures, Adv. Funct. Mater. 16 (2006) 1739–1744, https://doi.org/10.1002/adfm.200600394.
[25] S.L. Tao, K. Popat, T.A. Desai, Off-wafer fabrication and surface modification of asymmetric 3D SU-8 microparticles, Nat. Protoc. 1 (2007) 3153–3158, https://doi.org/10.1038/nprot.2006.451.
[26] B.L. Aekbote, J. Jacak, G.J. Schütz, E. Csányi, Z. Szegletes, P. Ormos, L. Kelemen, Aminosilane-based functionalization of two-photon polymerized 3D SU-8 microstructures, Eur. Polym. J. 48 (2012) 1745–1754, https://doi.org/10.1016/J.EURPOLYMJ.2012.06.011.
[27] R.A. Farrer, C.N. LaFratta, L. Li, J. Praino, M.J. Naughton, B.E.A. Saleh, M.C. Teich, J.T. Fourkas, Selective functionalization of 3-D polymer microstructures, J. Am. Chem. Soc. 128 (2006) 1796–1797, https://doi.org/10.1021/ja0583620.
[28] A.S. Quick, J. Fischer, B. Richter, T. Pauloehrl, V. Trouillet, M. Wegener, C. Barner-Kowollik, Preparation of reactive three-dimensional microstructures via direct laser writing and thiolene chemistry, Macromol. Rapid Commun. 34 (2013) 335–340, https://doi.org/10.1002/marc.201200796.
[29] D.W. Yee, M.D. Schulz, R.H. Grubbs, J.R. Greer, Functionalized 3D architected materials via thiol-Michael addition and two-photon lithography, Adv. Mater. 29 (2017) 1605293, https://doi.org/10.1002/adma.201605293.
[30] J. Glückstad, Optical manipulation: Sculpting the object, Nat. Photonics 5 (2011) 7–8, https://doi.org/10.1038/nphoton.2010.301.
[31] M.H. Jacobsen, T. Koch, Method of Photochemical Immobilization of Ligands Using Quinones, US6033784A, https://patents.google.com/patent/US6033784A/en 2000.
[32] C.A. Schneider, W.S. Rasband, K.W. Eliceiri, NIH image to imageJ: 25 years of image analysis, Nat. Methods 9 (2012) 671–675, https://doi.org/10.1038/nmeth.2089.
[33] D. Palima, T.B. Lindballe, M.V. Kristensen, S. Tauro, H. Stapelfeldt, S.R. Keiding, J. Glückstad, Alternative modes for optical trapping and manipulation using counter-propagating shaped beams, J. Opt. 13 (2011), 044013. https://doi.org/10.1088/2040-8978/13/4/044013.
[34] A. Bañas, O. Kopylov, M. Villangca, D. Palima, J. Glückstad, GPC Light Shaper: static and dynamic experimental demonstrations, Opt. Express 22 (2014) 23759–23769, https://doi.org/10.1364/OE.22.023759.
[35] G. Blagoi, S. Keller, F. Persson, A. Boisen, M.H. Jakobsen, Photochemical modification and patterning of SU-8 using anthraquinone photolinkers, Langmuir 24 (2008) 9929–9932, https://doi.org/10.1021/la800948w.
[36] T. Koch, N. Jacobsen, J. Fensholdt, U. Boas, M. Fenger, M.H. Jakobsen, Photochemical immobilization of anthraquinone conjugated oligonucleotides and PCR amplicons on solid surfaces, Bioconjug. Chem. 11 (2000) 474–483, https://doi.org/10.1021/BC000011H.
[37] J.Y. Lock, T.L. Carlson, R.L. Carrier, Mucus models to evaluate the diffusion of drugs and particles, Adv. Drug Deliv. Rev. 124 (2017) 34–49, https://doi.org/10.1016/j.addr.2017.11.001.
[38] J. Kočevar-Nared, J. Kristl, J. Šmid-Korbar, Comparative rheological investigation of crude gastric mucin and natural gastric mucus, Biomaterials 18 (1997) 677–681, https://doi.org/10.1016/S0142-9612(96)00180-9.
[39] J. Perez-Vilar, R.L. Hill, The structure and assembly of secreted mucins, J. Biol. Chem. 274 (1999) 31751–31754, https://doi.org/10.1074/jbc.274.45.31751.
[40] G.E. Yakubov, A. Papagiannopoulos, E. Rat, R.L. Easton, T.A. Waigh, Molecular structure and rheological properties of short-side-chain heavily glycosylated porcine stomach mucin, Biomacromolecules 8 (2007) 3467–3477, https://doi.org/10.1021/bm700607w.
[41] A. Bañas, D. Palima, M. Villangca, T. Aabo, J. Glückstad, GPC light shaper for speckle-free one- and two- photon contiguous pattern excitation, Opt. Express 7102 (2014) 5299–5310, https://doi.org/10.1364/OE.22.005299.
[42] P.J. Rodrigo, I.R. Perch-Nielsen, J. Glückstad, Three-dimensional forces in GPC-based counterpropagating-beam traps, Opt. Express 14 (2006) 5812–5822, https://doi.org/10.1364/OE.14.005812.
[43] H.-U. Ulriksen, J. Thogersen, S. Keiding, I.R. Perch-Nielsen, J.S. Dam, D.Z. Palima, H. Stapelfeldt, J. Glückstad, Independent trapping, manipulation and characterization by an all-optical biophotonics workstation, J. Eur. Opt. Soc. Rapid Publ. 3 (2008) 08034, https://doi.org/10.2971/jeos.2008.08034.
[44] V.R. Daria, R.L. Eriksen, S. Sinzinger, J. Glückstad, Optimizing the Generalized phase contrast method for a planar optical device, J. Opt. A Pure Appl. Opt. 5 (2003) S211–S215, https://doi.org/10.1088/1464-4258/5/5/367.
[45] M.J. Villangca, A. Bañas, D. Palima, J. Glückstad, Generalized phase contrast-enhanced diffractive coupling to light-driven microtools, Opt. Eng. 54 (2015) 111308, https://doi.org/10.1117/1.OE.54.11.111308.
[46] R.L. Eriksen, P.C. Mogensen, J. Glückstad, Demonstration of ternary-phase-array illumination based on the generalised phase contrast method, Opt. Commun. 202 (2002) 37–45, https://doi.org/10.1016/S0030-4018(02)01075-1.